

Xylan Structure and Dynamics in Native *Brachypodium* Grass Cell Walls Investigated by Solid-State NMR Spectroscopy

Pu Duan, Samuel J. Kaser, Jan J. Lyczakowski, Pyae Phyo, Theodora Tryfona, Paul Dupree,* and Mei Hong*

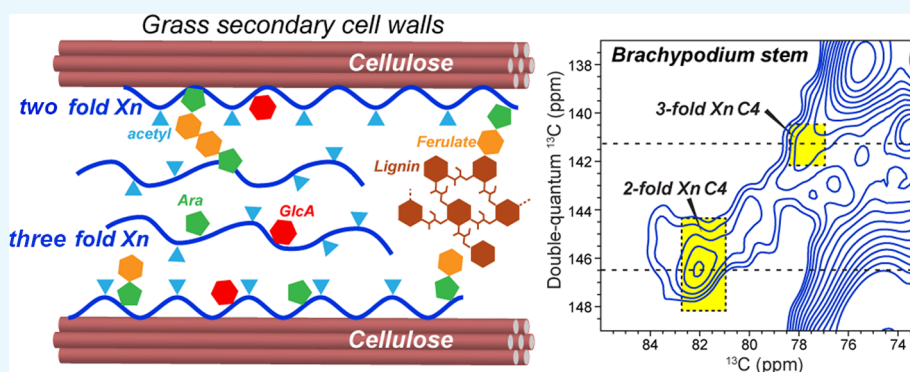
Cite This: <https://doi.org/10.1021/acsomega.1c01978>

Read Online

ACCESS |

Metrics & More

Article Recommendations



ABSTRACT: The polysaccharide composition and dynamics of the intact stem and leaf cell walls of the model grass *Brachypodium distachyon* are investigated to understand how developmental stage affects the polysaccharide structure of grass cell walls. ¹³C enrichment of the entire plant allowed detailed analysis of the xylan structure, side-chain functionalization, dynamics, and interaction with cellulose using magic-angle-spinning solid-state NMR spectroscopy. Quantitative one-dimensional ¹³C NMR spectra and two-dimensional ¹³C–¹³C correlation spectra indicate that stem and leaf cell walls contain less pectic polysaccharides compared to previously studied seedling primary cell walls. Between the stem and the leaf, the secondary cell wall-rich stem contains more xylan and more cellulose compared to the leaf. Moreover, the xylan chains are about twofold more acetylated and about 60% more ferulated in the stem. These highly acetylated and ferulated xylan chains adopt a twofold conformation more prevalently and interact more extensively with cellulose. These results support the notion that acetylated xylan is found more in the twofold screw conformation, which preferentially binds cellulose. This in turn promotes cellulose–lignin interactions that are essential for the formation of the secondary cell wall.

INTRODUCTION

For centuries, humans have relied on plant biopolymers as an essential food and animal feed source and for many economic activities such as housing and construction using the lignocellulose in timber. Recently, converting plant biomass into renewable chemical feedstocks and energy sources has attracted significant interest, as our society seeks to reduce the dependency on nonrenewable fossil fuels to address the challenge of global warming.^{1,2} The cell walls of commodity crops such as corn and many grass species are rich deposits of cellulose and hemicellulose, which can be converted into ethanolic biofuels.³ Grass cell walls are exceptionally rich in the hemicellulose glucuronoarabinoxylan (GAX), which accounts for as much as 50% of grass cell walls.⁴ However, these plant cell walls are also enriched in chemically recalcitrant components such as lignin, which need to be removed in order to convert the polysaccharides to fuel. Thus, a molecular

understanding of the plant cell wall composition and interactions between wall biopolymers is important for agriculture and the bioenergy economy. *Brachypodium distachyon* is a monocotyledonous grass in the same family (Poaceae) as wheat, corn, rice, and other crops. It has a short lifecycle and a small, well-characterized genome, making it amenable to the study of gene functions using genetic manipulation.⁵ Therefore, it is an excellent model plant for grass cell wall structural characterization.

Received: April 13, 2021

Accepted: May 21, 2021

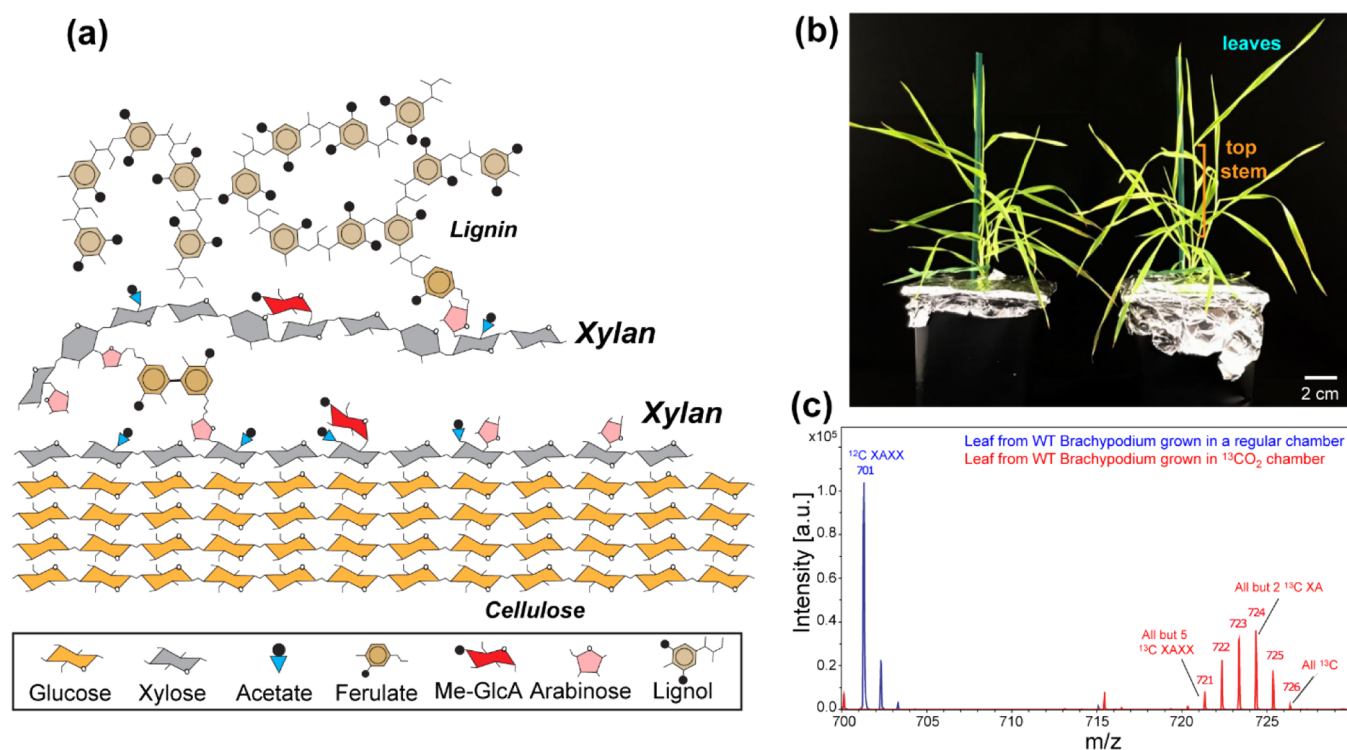


Figure 1. (a) Schematic of the key polymers in grass secondary cell walls and proposed intermolecular interactions. Xylan (gray) in the twofold conformation interacts with cellulose, while threefold xylan might fill the interfibrillar space. (b) Wild-type *Brachypodium distachyon* grown in hydroponics in the ^{13}C enrichment chamber. Three samples were harvested: leaves, top stem, and root. Photograph courtesy of Dr. Henry Temple. (c) MALDI mass spectrum of xylan from *Brachypodium* leaves. Data for plants grown in atmospheric conditions are shown in blue, while plants grown in $^{13}\text{CO}_2$ -enriched conditions are shown in red. The material was digested with xylanase GH11 to release xylotetraose with one arabinose branch (XAXX). The analysis of peak intensity indicates that xylan in the enriched material is >90% ^{13}C labeled.

Most grasses have two types of cell walls. The ubiquitous primary cell wall (PCW) provides mechanical support to plants while maintaining physical adaptability to accommodate cell growth and reproduction. The secondary cell wall develops as the tissue matures and is chemically recalcitrant and structurally rigid. While both cell walls contain cellulose and hemicelluloses, only the secondary cell wall contains lignin, a heavily cross-linked hydrophobic polyaromatic compound. Lignin interacts with cellulose fibrils through GAX, which is composed of a β -(1,4)-xylan backbone that is decorated with glucuronic acid and arabinose side chains (Figure 1a). The arabinose side chain can be further attached to ferulic acid (FA), which in turn crosslinks with lignin.⁶ While PCWs grow on the surface of all plant cells, secondary cell walls are deposited only in certain types of plant tissues during the course of plant development. For grass, stems account for most of the secondary cell wall.⁷ Comparative studies of the cell wall compositions of *Brachypodium* organs⁸ found that stems had substantially higher masses of lignin and ester- and ether-linked phenolics per gram of cell walls compared to leaves, as measured by acetyl bromide.⁹ The same study also measured the neutral monosaccharide content using Saeman hydrolysis¹⁰ and found a much higher concentration of glucose and xylose in extracts of the stem than in the leaves. These results indicate that the stem has more secondary cell walls than the leaf.

In addition to glucuronic acid and arabinose, xylan in plant cell walls is also decorated with acetate groups. NMR and mass spectrometry data indicate that xylans in *Arabidopsis thaliana* cell walls are acetylated on alternate xylosyl residues at the C2 or C3 positions.¹¹ Molecular dynamics simulations suggest that

this alternating acetylation pattern may promote a twofold screw conformation of xylan (Xn^{2f}), which may favor binding to cellulose owing to the steric availability of one side of the xylan chain. This twofold screw conformation differs from the threefold screw conformation (Xn^{3f}) adopted by unacetylated xylan in solution.¹² This hypothesis was confirmed by solid-state NMR data of the *Arabidopsis* stem, which showed cross peaks between Xn^{2f} and cellulose chemical shifts in two-dimensional (2D) ^{13}C correlation spectra.^{13,14} Quartz crystalline microbalance-dissipation experiments¹⁵ showed that acetylated xylan deposited more densely onto the cellulose surface than deacetylated xylan, and the deposited layer excluded water better, indicating that the acetylated xylan packs onto the cellulose surface more efficiently than deacetylated xylan. More recently, solid-state NMR spectra of maize, rice, switchgrass, and *Arabidopsis* stem cell walls¹⁶ showed numerous correlation peaks between lignin and Xn^{3f} , between lignin and a distorted conformation of Xn^{2f} , but not between lignin and cellulose. These data therefore suggest that cellulose and lignin may be bridged by xylan in certain conformations.¹⁶

Despite these advances in our understanding of xylan interactions with other wall polysaccharides, to date, no study has probed how xylan–cellulose interactions change with developmental stage. It is not known how primary wall versus secondary wall contents affect the xylan structure, dynamics, functionalization, and interaction with other wall polysaccharides. Here, we address this question by comparing the stem and leaf cell walls of the model grass *Brachypodium distachyon* (Figure 1b). Stems and leaves possess the most and the least

proportion of cells with the secondary cell wall, respectively, in *Brachypodium*. We examine undigested and never-dried whole-cell samples that preserve the native cell wall as well as the intracellular material. We employ magic-angle-spinning (MAS) solid-state NMR spectroscopy to obtain molecular-level structural and dynamical information. MAS NMR is a powerful nonperturbing atomic technique to analyze insoluble biological mixtures such as plant cell walls.¹⁷ It allows simultaneous studies of the chemical composition, three-dimensional packing, and dynamics of wall polysaccharides. Using solid-state NMR, we previously discovered extensive cellulose–pectin interactions in the PCWs of *Arabidopsis thaliana*, characterized the dynamics and hydration of the wall polysaccharides,^{18–20} and correlated these parameters with cell wall pH²¹ and the growth stage of *Arabidopsis* inflorescence.²² These studies established the central role of cellulose–pectin interactions in the PCW structure. We now address whether xylan plays a similar role in influencing the secondary cell wall development and the growth of grasses through its interactions with cellulose.^{13,16,23} We compare the ¹³C chemical shifts of whole stem and leaf samples with the ¹³C chemical shifts of *Brachypodium* PCWs extracted from seedlings,^{24,25} which have minimal amounts of secondary cell walls. These studies lead to a new model of the relationship among xylan functionalization, dynamics, and interaction with other wall biopolymers.

MATERIALS AND METHODS

Brachypodium Cell Wall Growth and ¹³C Labeling. *B. distachyon* seeds were surface-sterilized with a wash in 96% ethanol (1 min), followed by a wash in 20% bleach supplemented with Triton X-100 to a concentration of 0.01% (2 min). Seeds were rinsed in sterile distilled water three times and placed on 1/2 MS solid medium supplemented with 1% sucrose. The plants were grown for 2 weeks under long-day conditions (16 h light/8 h dark) at 21 °C. Two-week-old plants were transferred from MS plates to hydroponics pots. For hydroponics growth, a rockwool substrate (Cultilene, OptimaXX slabs) and an in-house growth medium [2 mM MgSO₄, 2 mM Ca(NO₃)₂, 50 μM FeEDTA, 5 mM KNO₃, 2.5 mM K₂HPO₄, and KH₂PO₄ buffer, pH 5.5, 70 μM H₃BO₃, 14 μM MnCl₂, 0.5 μM CuCO₄, 1 μM ZnSO₄, 0.2 μM NaMoO₄, 10 μM NaCl, and 0.1 μM CoCl₂] were used.

Plants in hydroponics pots were placed in a sealed ¹³C enrichment chamber and grown for 5 weeks as previously described.¹³ Briefly, the chamber is a climate-control unit into which air stripped of ¹²CO₂ and amended with ¹³CO₂ (Cambridge Isotope Laboratories, MA, USA) is pumped. The growth in the ¹³C enrichment chamber was performed at 23 °C between 65 and 75% relative humidity levels. Long-day conditions (16 h light/8 h dark) were used during the ¹³C growth. After 5 weeks of growth in the ¹³C enrichment chamber, the 24 plants were harvested, sectioned, and snap frozen in liquid nitrogen. The plant material was stored at –80 °C before the solid-state NMR analysis. Matrix-assisted laser desorption ionization (MALDI) mass spectra indicate a ¹³C enrichment level of >90% (Figure 1c).

Solid-State NMR Experiments. ¹³C-labeled *Brachypodium* tissues were packed into 3.2 mm MAS rotors using a funnel and packer. Three samples were measured in this study: a stem sample, a leaf sample, and a root sample. The hydrated sample masses range from 30 to 50 mg, and experiments were conducted at a set temperature of 275 K, which corresponds to

a sample temperature of about 285 K. This moderately low temperature was chosen to minimize the enzymatic digestion of these whole-cell samples.

All MAS NMR spectra were measured on an 800 MHz (18.8 T) and a 600 MHz (14.1 T) Bruker Avance II spectrometer. The MAS frequencies range from 9 to 12 kHz. Typical radiofrequency (rf) field strengths were 50 and 71.4 kHz for ¹³C and ¹H, respectively. Proton decoupling was carried out using the two-pulse phase-modulation²⁶ scheme with an rf field strength of 71.4 kHz. ¹³C chemical shifts were externally referenced to the adamantane methylene peak at 38.48 ppm on the tetramethylsilane scale.

Four types of one-dimensional (1D) ¹³C NMR spectra were measured. A quantitative direct polarization (DP) experiment used a ¹³C 90° pulse to excite the ¹³C magnetization and a long recycle delay of 35 s to ensure full spin–lattice (*T*₁) relaxation of the ¹³C magnetization. This experiment gives intensities that quantitatively reflect the relative abundance of polysaccharides in the sample. Another ¹³C DP experiment used a short recycle delay of 2 s to preferentially suppress the signals of rigid molecules with slow *T*₁ relaxation while enhancing the signals of dynamic molecules with fast ¹³C *T*₁ relaxation. The third 1D ¹³C experiment is refocused insensitive nuclei enhancement by polarization transfer (INEPT), which detects ¹³C magnetization transferred from ¹H spins via *J* coupling. The total polarization transfer time was 6 ms, consisting of two delays of 1.8 ms, followed by another two delays of 1.2 ms. These values correspond to 1/(4*J*_{CH}) and 1/(6*J*_{CH}), respectively, based on the typical one-bond ¹³C–¹H *J* coupling of 140 Hz.²⁷ The refocused INEPT spectra preferentially detect highly dynamic molecules such as matrix polysaccharides, monosaccharides, and proteins in solution. Finally, a ¹³C cross-polarization (CP) experiment was conducted to selectively detect rigid molecules such as cellulose. The CP experiment used a contact time of 0.75 ms and 70–100% of rf amplitude ramp on the ¹H channel.

To resolve the multiple polysaccharide signals in these native plant tissues, we measured two types of 2D ¹³C–¹³C double-quantum and single-quantum correlation spectra (INADEQUATE). The first type utilized 0.75 ms ¹H–¹³C CP to generate the initial ¹³C polarization and relied on the SPC-5 sequence²⁸ to recouple the ¹³C–¹³C dipolar coupling that is averaged by MAS. This CP-INADEQUATE experiment selectively detects rigid polysaccharides and was carried out on the 600 MHz spectrometer under 9.8 kHz MAS. The indirect dimension had a spectral width of 195 ppm and was sampled with 292*t*₁ increments. The numbers of scans per *t*₁ increment were 192, 280, and 528 for the stem, leaf, and root samples, respectively. We also measured 2D-refocused *J*-INADEQUATE spectra²⁹ using ¹³C DP and a short recycle delay of 2 s, which preferentially detect mobile molecules. The total *J*-coupling evolution period was 2 × 3 = 6 ms. These *J*-INADEQUATE experiments were conducted on the 800 MHz spectrometer under 12 kHz MAS, with 80 ppm spectral width for the indirect dimension and 350*t*₁ increments. The numbers of scans per *t*₁ increment were 64, 224, and 544 for the stem, leaf, and root samples, respectively.

Complementing the 2D INADEQUATE spectra, we measured 2D ¹³C–¹³C spin–diffusion correlation spectra to detect intramolecular and intermolecular contacts. Spin–diffusion mixing allows the observation of polysaccharides with intermediate mobilities, which are preferentially suppressed in both the CP- and *J*-INADEQUATE spectra. We

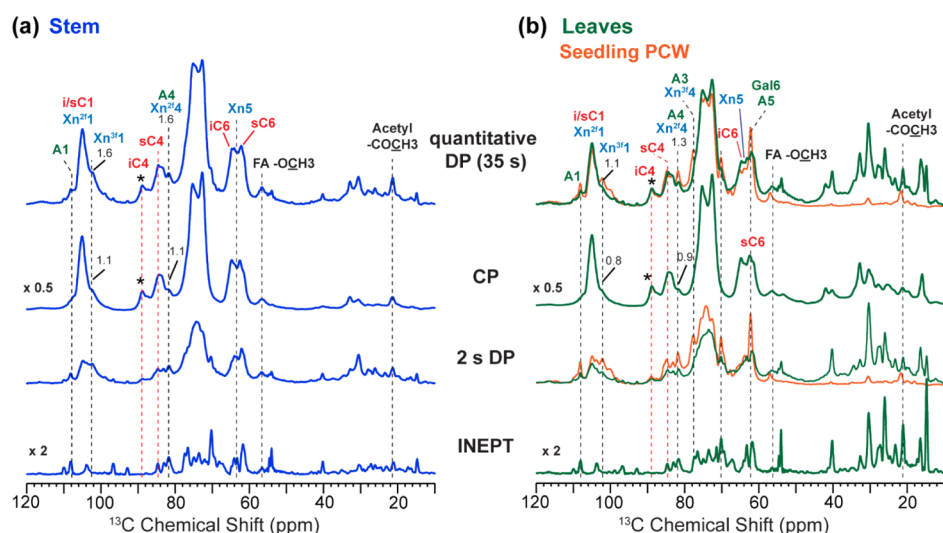


Figure 2. 1D ^{13}C NMR spectra of *Brachypodium distachyon* whole cells. (a) Stem spectra. (b) Leaf spectra (green), which are overlaid with the spectra of extracted seedling PCWs (orange). From top to bottom: quantitative ^{13}C spectra measured with a 35 s recycle delay; CP spectra; DP spectra measured with a 2 s recycle delay; and INEPT spectra. Spectra of stem and leaf samples are scaled relative to each other to have the same 89 ppm peak intensities in the 35 s DP. The same scaling factor was applied to all spectra of each sample. The seedling sample's spectra are also scaled to match the 89 ppm intensity with the leaf sample in the quantitative DP spectra. Additional scaling factors are applied to the CP and INEPT spectra for clarity. Asterisks indicate the interior cellulose C4 peak, whose intensity is used to normalize other peak intensities. Note the higher xylan peak intensities in the stem spectra than in the leaf spectrum. These are shown at 103 ppm for Xn^{3f} C1 and 82 ppm for Xn^{2f} C4.

used a 30 ms COmbined R2n(v)-Driven (CORD)³⁰ sequence to detect predominantly intramolecular correlations and 1 s ^{13}C spin diffusion to observe both intramolecular and intermolecular correlations. The latter consists of 300 ms CORD mixing and 700 ms ^1H -driven spin diffusion. The 30 ms 2D CC spectrum of the stem sample was measured under 9.8 kHz MAS with 88 scans of signal averaging per t_1 slice, while the corresponding leaf spectrum was measured under 11.4 kHz MAS with 80 scans of signal averaging. The 1 s 2D CC spectra were measured on the 600 MHz spectrometer under 12 kHz MAS, with 160 and 184 scans of signal averaging for the stem and leaf samples, respectively. For all 2D CC experiments, the indirect dimension has a spectral width of 200 ppm and was measured with $360t_1$ increments.

To investigate polysaccharide dynamics, we measured dipolar-doubled 2D ^1H - ^{13}C dipolar chemical-shift (DIPSHIFT) correlation spectra^{31,32} on the 800 MHz spectrometer under 9.2 kHz MAS. ^1H - ^1H homonuclear decoupling was achieved using the frequency-switched Lee-Goldburg sequence, which has a scaling factor of 0.577.³³ Both quantitative DP-DIPSHIFT and CP-DIPSHIFT experiments were conducted, which evaluate the mobility of all polysaccharides and the more rigid polysaccharides, respectively. The DIPSHIFT dephasing curves were fitted using a custom-written Fortran program to obtain the dipolar coupling strengths. The fit values were divided by 23 kHz, the rigid-limit one-bond C-H dipolar coupling,³⁴ to obtain the order parameter S_{CH} .

RESULTS

The ^{13}C -labeled whole-cell *Brachypodium* samples analyzed in this work differ from the previously investigated seedling PCW²⁴ in three ways. First, the current samples were grown in two stages over a long period of 7 weeks, during which mature stems and leaves were obtained (Figure 1b). Second, the plants were ^{13}C -enriched using $^{13}\text{CO}_2$ under light conditions, in contrast to the previous ^{13}C -glucose labeling of the seedlings in the dark. Third, we collected roots, top stems, and leaves

without any processing in order to preserve the cell wall architecture. The samples were stored at -80°C until NMR experiments. The peak intensities in the mass spectra (Figure 1c) indicate that the ^{13}C enrichment level is greater than 90%.

Polysaccharide Compositions of *Brachypodium* Stem and Leaf Cell Walls. Previous chemical analysis of the chemical composition of *Brachypodium* tissues revealed that the stem has substantially higher lignin and ester- and ether-linked phenolic contents⁸ and higher concentrations of glucose and xylose¹⁰ than leaves, indicating that the stem has more secondary cell walls. We first verified this compositional difference in our samples by measuring four types of 1D ^{13}C NMR spectra for the stem and leaf samples (Figure 2). These spectra include a quantitative DP spectrum, a CP spectrum, a 2 s DP spectrum, and an INEPT spectrum. Together, these spectra allow us to compare the polysaccharide composition and dynamics of these two tissues. In all ^{13}C spectra, the protein and lipid peaks in the 10–45 ppm range are more intense in the leaf than in the stem, indicating that wall polysaccharides account for a smaller fraction of the total plant material in the leaf than in the stem. Specifically, the intensities of the 50–120 ppm region of the quantitative ^{13}C spectra represent 73% of the total spectral intensities for the stem but only 53% for the leaf. This difference is consistent with previous chemical analysis that showed the stem to have thicker cell walls than leaf.⁸ The lipid and protein intensities are the strongest in the INEPT spectrum of the leaf and the weakest in the INEPT spectrum of the stem, indicating that the lipids and proteins are highly dynamic in the leaf. Within the polysaccharide region of the ^{13}C spectra, normalized by the resolved crystalline interior cellulose iC4 peak at 89 ppm in the 35 s DP spectra, the 103 ppm Xn^{3f} C1 peak and the 82 ppm Xn^{2f} C4 peak exhibit higher intensities in the stem than in the leaf in both the quantitative DP and CP spectra, indicating that there is a higher percentage of xylan in the stem than in the leaf. Since the grass secondary cell wall has a higher GAX content than grass PCW,⁴ the higher xylan concentration of

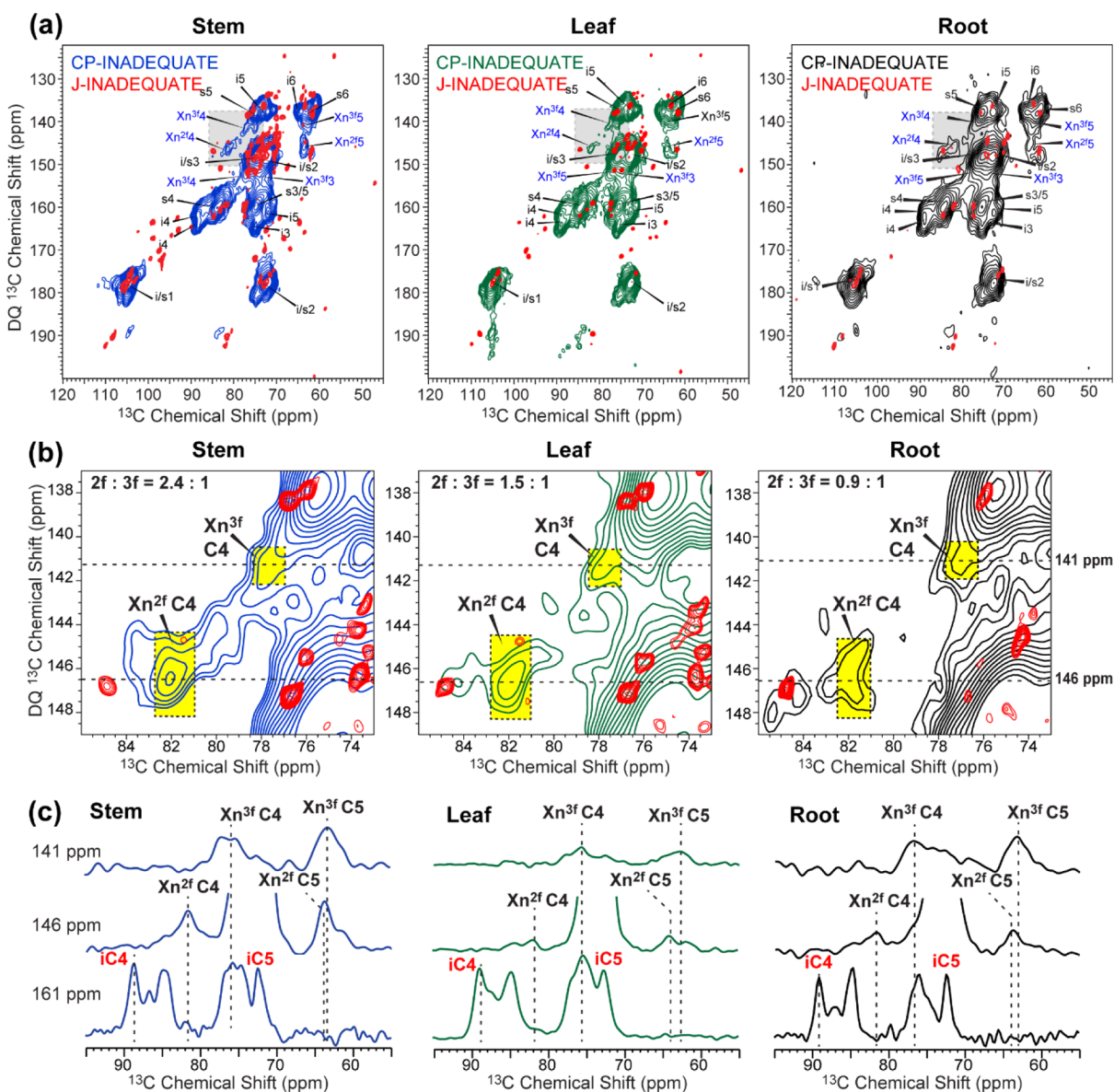


Figure 3. 2D ^{13}C – ^{13}C INADEQUATE spectra of *Brachypodium* cell walls. From left to right: stem, leaves, and root. Red: J-INADEQUATE spectra. Other colors: CP-INADEQUATE spectra. (a) Full carbohydrate region of the 2D spectra. The CP-INADEQUATE peaks have much broader linewidths due to the preferential detection of rigid polysaccharides. The J-INADEQUATE spectra show narrow peaks due to the selective detection of highly dynamic matrix polysaccharides. (b) Zoomed-in area with DQ chemical shifts of 137–148 ppm, showing the characteristic Xn^{2f} and Xn^{3f} C4 peaks. Integration areas are highlighted in yellow. The relative peak intensities indicate that the $\text{Xn}^{2f}/\text{Xn}^{3f}$ concentration ratios are the highest in the stem and the lowest in the root cell wall. (c) 1D ^{13}C cross sections at DQ chemical shifts of 141, 146, and 161 ppm, corresponding to Xn^{3f} , Xn^{2f} , and interior cellulose correlation peaks, respectively. Intensities are normalized to the 161 ppm cross section within each sample.

the stem indicates a greater proportion of secondary cell walls in the stem than in the leaf.

We also compared the leaf spectra with the previously measured spectra of seedling PCW²⁴ (Figure 2b). The seedling PCW spectra show much lower protein and lipid signals, consistent with the mild extraction procedure used to prepare the sample and the lack of the intracellular content. In the polysaccharide region of the spectra, the arabinose content is higher in the extracted seedling PCW than in the leaf samples, as evidenced by the higher intensities of the 108, 82, and 78 ppm peaks in the quantitative DP and 2 s DP spectra of the seedling sample compared to the leaf. These intensity differences are consistent with higher amounts of pectic arabinans and/or xylan in the seedling than in the leaf cell wall.

Different Xylan Contents between Stem and Leaf. To further resolve the ^{13}C chemical shifts of the wall polysaccharides, we measured 2D INADEQUATE correlation spectra. Figure 3 compares the 2D J- and CP-INADEQUATE spectra of the stem, leaf, and root tissues. The J-INADEQUATE spectra preferentially detect dynamic polysaccharides, whereas the CP-INADEQUATE spectra preferentially detect immobilized and rigid polysaccharides. The J-INADEQUATE spectra of all three *Brachypodium* samples (stem, leaf, and root) have much lower intensities than the previously reported seedling PCW spectra (Figure 4).²⁴ Surprisingly, more than half of the arabinose signals in the seedling PCW become undetectable in both the stem and leaf samples. Most of these missing signals belong to branched or terminal arabinose such as *t*-Ara in GAX (A^d), with C1 and C2

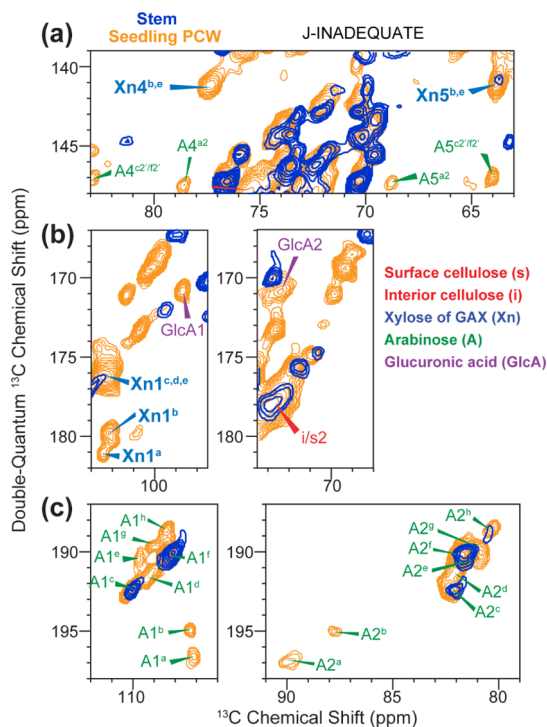


Figure 4. Selected regions of the 2D ^{13}C *J*-INADEQUATE spectra of the *Brachypodium* stem (blue) and seedling PCWs (orange). (a) DQ chemical shifts from 139 to 148 ppm, showing xylan C4–C5 correlations and some of the arabinose C4–C5 correlations. (b) DQ chemical shifts from 167 to 182 ppm, showing xylan C1 and GlcA C1–C2 correlations. (c) DQ chemical shifts of 187–198 ppm, showing arabinose C1–C2 correlations.

chemical shifts of 109 and 82 ppm,²⁴ respectively (Figure 4c), indicating that the xylan chains in the stem and leaf do not contain as many dynamic arabinose rings. Two types of arabinose residues, A^c and A^f , remain dynamic in the stem and are detected in the *J*-INADEQUATE spectra. Various dynamic glucuronic acid (GlcA) residues that were previously observed in the seedling PCW²⁴ are also missing in the stem and leaf, as seen by the absence of C1 and C2 chemical shifts of 99 and 72 ppm, respectively, in the *J*-INADEQUATE spectra (Figure 4b). Finally, the xylan backbone signals have lower intensities in the whole-cell spectra than in the seedling PCW spectra. For example, no Xn^{3f} C4 peak (141, 77) ppm is detected in the whole-cell samples (Figure 4a), and the xylan C1 signal at (178, 102) ppm is also missing. Here, we denote all peak positions in the 2D NMR spectra in the order of the chemical shifts in the first and second dimension, (ω_1 , ω_2). The pronounced intensity drop of the *J*-INADEQUATE spectra of the whole stem and leaf samples indicates that these whole cells contain lower levels of matrix polysaccharides compared to the seedling PCWs and/or contain less dynamic matrix polysaccharides.

To investigate whether it is the matrix polysaccharide concentration or the dynamics that changed between the seedling PCWs and the stem and leaf cell walls, we measured 2D CP-INADEQUATE spectra. We focus on the xylan signals, which are absent in the *J*-INADEQUATE spectra. As expected, the CP-INADEQUATE spectra are dominated by the signals of cellulose and feature much broader peaks than the *J*-INADEQUATE spectra due to the preferential detection of rigid polysaccharides. Xn^{2f} and Xn^{3f} signals are now observed at

double-quantum (DQ) chemical shifts of 146 and 141 ppm, respectively, in the stem, leaf, and root spectra (Figure 3a). These cross sections show xylan C4–C5 correlation peaks and are well resolved from the cellulose peaks. The zoomed-in areas between DQ chemical shifts of 137 and 149 ppm (Figure 3b) highlight the absence of these rigid xylans' C4 peaks from the *J*-INADEQUATE spectra. Integration of the Xn^{2f} and Xn^{3f} C4 peak intensities (yellow highlighted areas) indicates that the stem has the highest ratio of rigid Xn^{2f} to Xn^{3f} concentrations, while the root has the lowest. Comparing the xylan cross sections with the 161 ppm cross section of the cellulose C4–C5 correlation peaks, we estimated the relative concentrations of these rigid xylans among the three tissues. It is important to note that the CP-INADEQUATE experiment preferentially detects highly rigid molecules, thus the intensity differences among these spectra reflect the concentration differences of the most rigid xylans rather than all xylans in the cell wall. Normalized to the cellulose intensities, we find that the stem has 2 times higher Xn^{3f} C4 intensity than leaf and 3 times higher Xn^{2f} C4 intensity than the leaf (Figure 3c). Since the appearance of Xn^{2f} was previously found to be associated with cellulose binding,^{13,35} the higher Xn^{2f} concentration in the stem suggests that there are more GAX–cellulose contacts in the stem than in the leaf and root cell walls. The surface-to-interior cellulose intensity ratio in the 161 ppm cross section is very similar for all three tissues, indicating that cellulose fibrils have similar diameters and structures in these cell walls.³⁶ The similarity of cellulose structures in these three cell walls implies that the xylan structural and concentration changes may be more important than the cellulose structure for giving rise to different wall properties of these plant tissues.

2D *J*- and CP-INADEQUATE spectra reveal the signals of highly dynamic and highly rigid polysaccharides, respectively, but do not exhibit the signals of molecules with intermediate mobilities. To obtain more quantitative information about all polysaccharides in the cell wall, we measured 2D ^{13}C – ^{13}C correlation spectra with 30 ms spin diffusion mixing. Figure 5 shows the 2D spectra of the stem and leaf, together with key 1D cross sections extracted from various ω_1 chemical shifts. The cross sections are plotted to preserve their relative intensities in each 2D spectrum but scaled between the two 2D spectra such that the 50–110 ppm polysaccharide regions of the 2D spectra have the same integrated intensities. Therefore, the intensity differences between the stem and leaf samples in the 1D cross sections reflect the concentration differences of the polysaccharides.

The 89 ppm cross section of interior cellulose C4 confirms that the cellulose concentration is similar between the stem and leaf samples. Importantly, the resolved Xn^{2f} and Xn^{3f} signals are $\sim 20\%$ higher for the stem than those for the leaf, indicating that the GAX concentration in the stem is 1.2 times that of the leaf (Figure 5c). This difference is more moderate compared to the 3 times higher Xn^{2f} intensities observed in the stem CP-INADEQUATE spectra (Figure 3). We attribute this discrepancy to the fact that the 30 ms 2D CC spectra detect both rigid and partly mobile molecules, so that they reflect the total xylan populations in the cell wall rather than only highly rigid xylans. We also detected a characteristic C1–C2 correlation peak of *t*-Ara at (108, 82) ppm in both the stem and leaf spectra (Figure 5c). We assign this *t*-Ara to those associated with GAX based on the fact that these cross-peak intensities are within a factor of 2 of the xylan peak intensities in the 2D spectra. In *Brachypodium* seedling PCWs,²⁴ the GAX

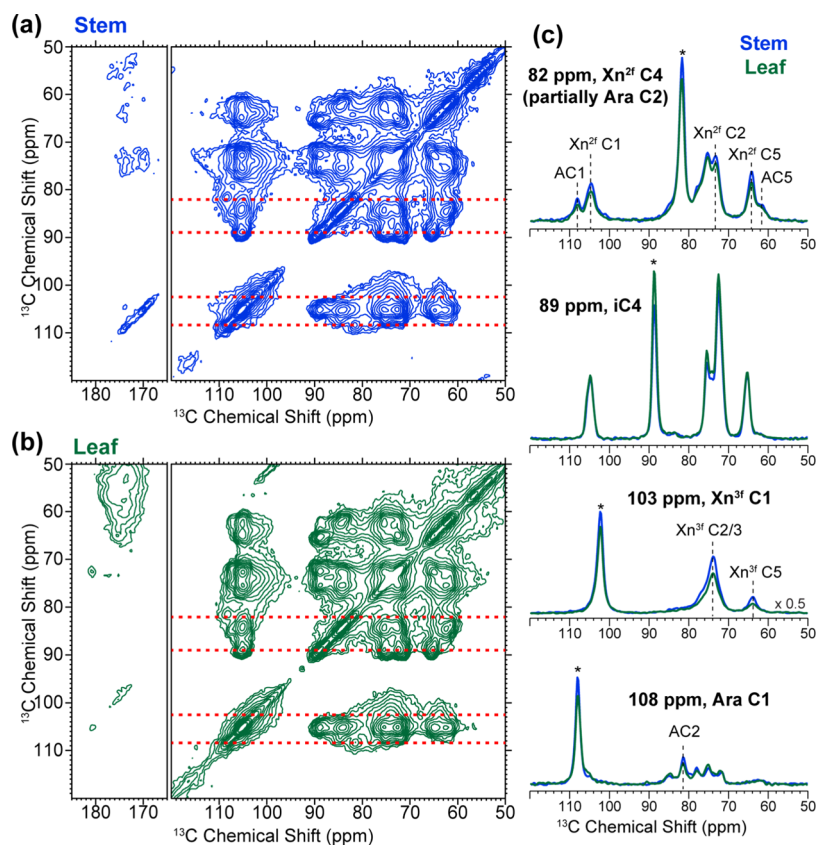


Figure 5. 2D ^{13}C – ^{13}C correlation spectra of *Brachypodium* whole cells with 30 ms ^{13}C spin diffusion mixing. (a) Stem spectrum. (b) Leaf spectrum. (c) Key 1D cross sections extracted at the indicated ω_1 chemical shifts of the stem (blue) and leaf (green) 2D spectra. The 2D spectra are scaled to have the same integrated intensities for the polysaccharide region (50–110 ppm) for the two samples, and the same scaling factor is applied to the corresponding cross sections. Asterisks indicate the diagonal peaks in each 1D cross section.

t-Ara (type d) has a C1 chemical shift of 109.2 ppm (Figure 4c). This chemical shift is absent in either the INADEQUATE spectra or the 2D ^{13}C – ^{13}C spin diffusion spectra of the stem and leaf samples. We tentatively attribute this chemical shift difference to a small conformational and/or mobility difference of GAX between the secondary cell walls of the stem and leaf and the PCWs.²⁴

Long-Range 2D ^{13}C Spin Diffusion Spectra Reveal the Chemical Functionalization of Xylan. To obtain information about the intermolecular interactions and side-chain functional groups that are not directly bonded to the backbone, we measured 2D ^{13}C – ^{13}C correlation spectra with a long mixing time of 1 s (Figure 6). Similar to the 30 ms spectra, we plotted the 1D cross sections of the 2D spectra to match the integrated intensities in the 50–110 ppm region of the two 2D spectra. Cross-peak intensity at chemical shifts of (ω_1, ω_2) represents the fraction of magnetization transferred from a carbon with a chemical shift of ω_1 to a second carbon with a chemical shift of ω_2 . When the cross peak is between two carbons that are covalently close, such as between the xylan backbone and side-chain carbons, then the (ω_1, ω_2) peak intensity reflects the percentage of the backbone that is decorated with a particular side chain.

Again, the 89 ppm cross section of interior crystalline cellulose C4 shows similar intensities between the stem and leaf spectra, indicating that the cellulose content is similar between the two whole-cell samples. In comparison, the 21 ppm cross section of acetyl CH_3 exhibits higher total intensities for the stem than for the leaf. Specifically, the acetyl cross

peaks with 82 ppm Xn^{2f} C4 and with 103 ppm Xn^{3f} C1 are 2.5 times higher for the stem than those for the leaf, indicating that the stem cell wall contains more acetylated Xn^{2f} and Xn^{3f} than the leaf. For comparison, the one-bond Xn^{2f} C4–C5 cross peak at (82, 64) ppm and the one-bond Xn^{3f} C1–C2 cross peak at (103, 73) ppm exhibit an intensity increase of $\sim 20\%$ for the stem compared to that for the leaf, consistent with the 30 ms 2D spin diffusion spectra. Note that the one-bond xylan cross peaks reflect the concentrations of all xylose residues in these samples, whereas the acetyl-xylan cross peaks in the 21 ppm cross section reflect the concentrations of acetylated xylose in xylans. Acetylated xylan is known to pack with cellulose fibrils better than unacetylated xylan¹⁵ and is thus more immobilized. Since the CP-INADEQUATE spectra also indicate 2–3 times more xylans in the stem than in the leaf, the CP-INADEQUATE spectra report the same information as the 21 ppm cross section of the 1 s CC spectra about the relative amount of rigid acetylated xylan in the two cell walls.

While the intensities of the 21 ppm acetyl cross section provide information about the total acetylated xylan in the cell walls, the 82 ppm cross section of Xn^{2f} C4 and the 103 ppm cross section of Xn^{3f} C1 provide information about the acetylation level of xylan. In the 82 ppm cross section, the 21 ppm acetyl cross peak is higher in the stem spectrum than that in the leaf spectrum. Normalized by the 82 ppm diagonal peak intensity, the acetyl cross peak's integrated intensity is 0.30 for the stem and is much lower (~ 0.08) for the leaf (shown next to the 21 ppm peak in Figure 6c). The 82 ppm peak in these CP-based 2D spectra mainly results from Xn^{2f} C4 and only a

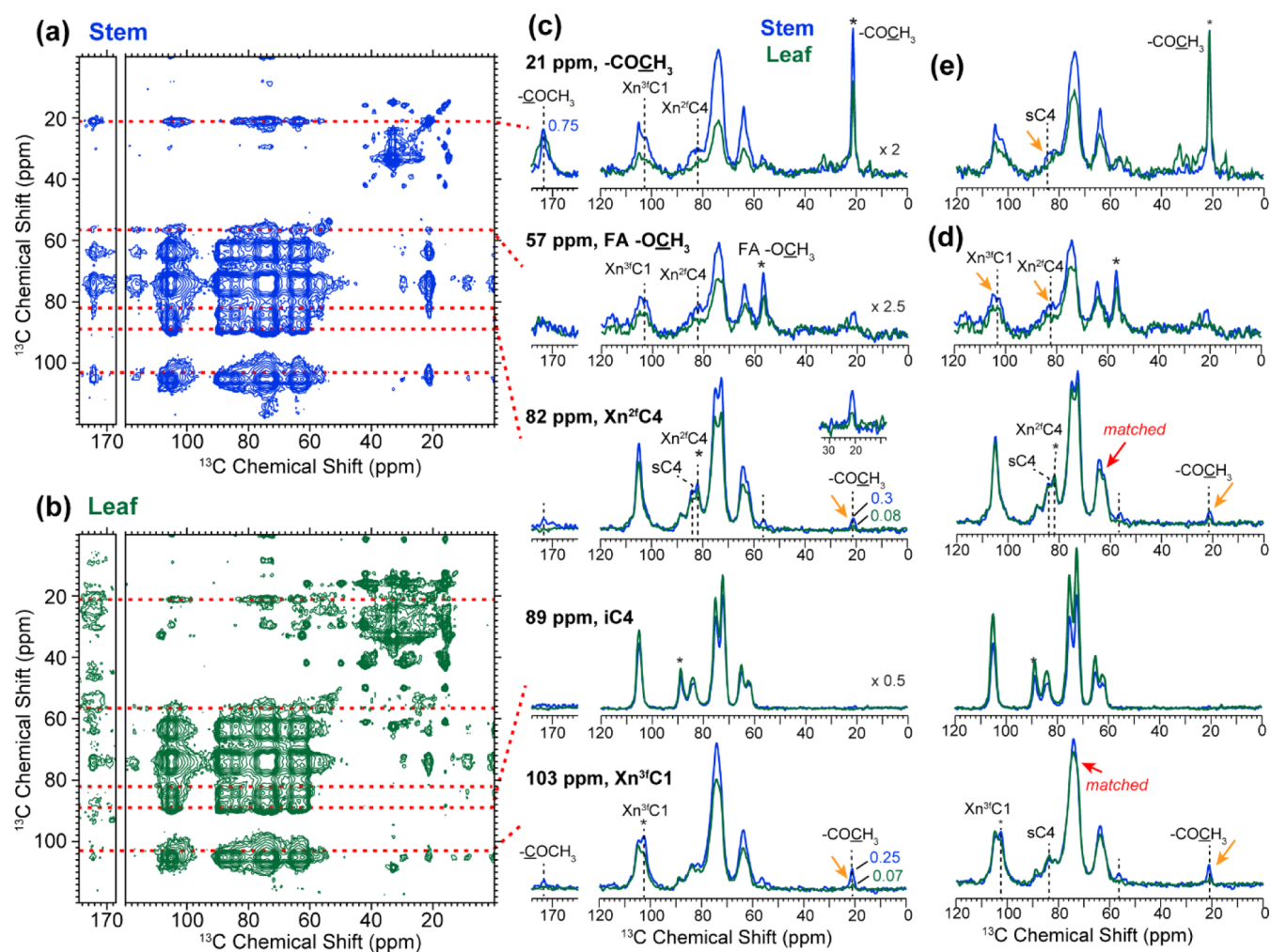


Figure 6. 2D ^{13}C – ^{13}C correlation spectra of *Brachypodium* whole cells with 1 s ^{13}C spin diffusion mixing. (a) Stem spectrum. (b) Leaf spectrum. (c) Key 1D row cross sections extracted at the indicated chemical shifts of the stem (blue) and leaf (green) 2D spectra. The 2D spectra are scaled to have the same integrated intensities for the polysaccharide region (50–110 ppm) for the two samples, and the same scaling factor is applied to the corresponding cross sections. Asterisks indicate the diagonal peaks in each 1D cross section. Numbers represent the intensity ratios of the cross peaks from the diagonal peak in each cross section. (d) The 57, 82, 89, and 103 ppm cross sections from (c), rescaled by raising the leaf spectral intensities 1.2-fold, so that the 64 ppm Xn^{2f} C4 peak in the 82 ppm cross section and the 73 ppm Xn^{3f} C2 peak in the 103 ppm cross section (red arrows) have the same intensities as the corresponding peaks in the stem spectra. In this way, it can be seen more clearly that the stem exhibits higher cross-peak intensities to the 21 ppm acetyl peak than the leaf (orange arrows), indicating that the xylan acetylation level is higher in the stem than in the leaf. (e) 21 ppm cross section from (c), where the leaf spectrum is scaled up to match the stem cell wall's 21 ppm peak. The orange arrow indicates that the stem has a higher cross peak to surface cellulose C4 compared to that in the leaf, indicating that the acetylated xylan contacts cellulose more in the stem than in the leaf cell wall.

minor fraction of the intensity results from Ara C2, and the relative contribution of the two species is expected to be similar between the stem and leaf. Thus, the cross-peak to diagonal-peak intensity ratio in the 82 ppm cross section mostly represents the fraction of magnetization transferred from the xylan backbone to the acetyl side chain. Thus, these different intensity ratios indicate that Xn^{2f} is more acetylated in the stem than in the leaf cell wall. Similarly, in the 103 ppm cross section of Xn^{3f} C1, the 21 ppm acetyl peak cross-peak intensity is higher in the stem than that in the leaf. To further visualize this acetylation difference, we scaled the 1D cross sections of the two samples to match their xylan cross-peak intensities at (82, 64) and (103, 73) ppm (Figure 6d). It can be seen that the intensities of Xn^{2f} C4—acetyl correlation at (82, 21) ppm and the Xn^{3f} C1—acetyl correlation at (103, 21) ppm remain higher in the stem than those in the leaf, indicating that both Xn^{2f} and Xn^{3f} are more acetylated in the

stem than in the leaf. These data, together with the 30 ms CC results, indicate that not only is the total xylan content higher (by $\sim 20\%$) in the stem than in the leaf, but also the xylan acetylation level is higher in the stem for both twofold and threefold xyans.

The 57 ppm cross section of the 1 s 2D CC spectra results from the methoxy groups of phenolic species such as FA and guaiacyl (G) or syringyl (S) groups in lignin. Since FA is covalently linked to xylan through the α -(1,3)-Araf-FA side chain of GAX, we assigned the methoxy signal to FA.²⁴ Thus, the (57, 82) and (57, 103) ppm cross peaks represent the fraction of magnetization transfer from FA to Xn^{2f} and Xn^{3f} . After scaling the 1D cross section of the two samples to match their xylan peak intensities (Figure 6d), we find that the ferulate cross peaks are $\sim 60\%$ higher in the stem than in the leaf spectra, indicating that the two xylan conformers are not

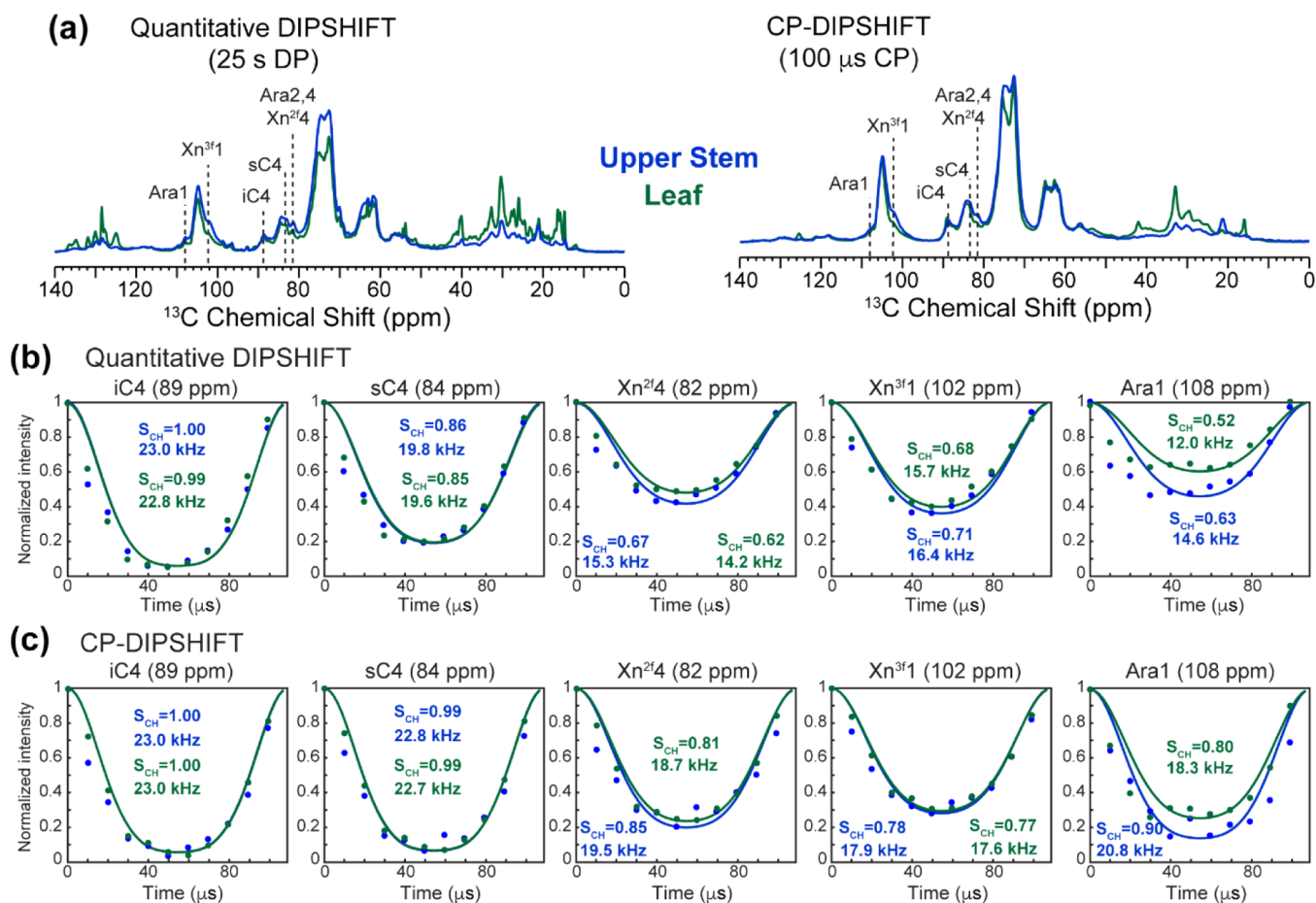


Figure 7. ^{13}C - ^1H dipolar-doubled DIPSHIFT spectra to measure polysaccharide dynamics in *Brachypodium*. Blue: stem data and green: leaf data. (a) ^{13}C quantitative DP spectra and CP spectra of the two samples, normalized by the total integrated area. Key ^{13}C signals of interest are assigned. (b) Quantitative ^{13}C - ^1H DIPSHIFT dipolar dephasing curves for representative ^{13}C sites. (c) CP-DIPSHIFT ^{13}C - ^1H dipolar dephasing curves for representative ^{13}C sites. The dipolar order parameters S_{CH} , obtained from best-fit simulations, are given in each panel.

only more acetylated but also more ferulated in the stem than in the leaf cell wall.

In the 82 ppm cross section of Xn^{2f} C4, the (82, 84) ppm cross peak to surface cellulose is higher in the stem than in the leaf. This is verified by the higher intensity of the 21 ppm acetyl correlation with the 84 ppm sC4 peak in the stem compared to that in the leaf (Figure 6e). In comparison, in the 103 ppm cross section of Xn^{3f} C1, the (103, 84) ppm cross peak of Xn^{3f} to surface cellulose has similar intensities between the two cell walls. These observations suggest that Xn^{2f} interacts more extensively with cellulose fibrils than Xn^{3f} in the stem cell wall.

Hemicelluloses and Matrix Polysaccharides Are Immobilized in the Stem. The different xylan intensities between stem and leaf cell walls in the 2D CP-INADEQUATE spectra and CC spectra suggest that xylan mobility might also differ between the two cell walls. To test this hypothesis, we measured C-H dipolar couplings using the DIPSHIFT experiment. Figure 7 shows the quantitative DP-DIPSHIFT and CP-DIPSHIFT spectra of the stem and leaf. The more rigid a molecule is, the stronger the dipolar coupling and the larger the dipolar order parameter S_{CH} . The larger dipolar coupling is manifested as a deeper DIPSHIFT oscillation, with lower intensities in the middle of the rotor period. Figure 7b shows that cellulose has similar rigidity between the stem and leaf, with strong dipolar couplings for the 89 and 84 ppm peaks

of the interior and surface cellulose C4. This is consistent with the unperturbed interior-to-surface cellulose intensity ratio found in the CP-INADEQUATE spectra. Both DP and CP DIPSHIFT spectra indicate that arabinose in stem and leaf cell walls is less mobile compared to that in the PCW ($S_{\text{CH}} = 0.41$).²⁴ This is consistent with the absence of *t*-Ara of GAX in the *J*-INADEQUATE spectra, which preferentially detects dynamic molecules. The Xn^{2f} mobility is manifested in the 82 ppm peak. The DP-DIPSHIFT spectra of this peak show smaller dipolar couplings than the CP-DIPSHIFT spectra. We attribute this difference to the partial overlap of the arabinan signal with the xylan signal in the DP spectra. Suppression of the arabinan signal by CP thus gives a more accurate report of the Xn^{2f} mobility. Figure 7c shows that Xn^{2f} is more rigid in the stem than in the leaf cell wall, which correlates with the higher Xn^{2f} acetylation level and more extensive xylan contact with cellulose. In comparison, Xn^{3f} shows similar mobility between stem and leaf cell walls, even though it is more acetylated and ferulated in the stem cell wall. This suggests that the mobility of xylan chains is influenced more by xylan interaction with cellulose rather than by acetylation and ferulation alone. Finally, Xn^{3f} is less rigid than Xn^{2f} in both stem and leaf cell walls, consistent with the view that Xn^{3f} is less efficiently immobilized by interactions with other cell wall components such as lignin and cellulose compared to Xn^{2f}.

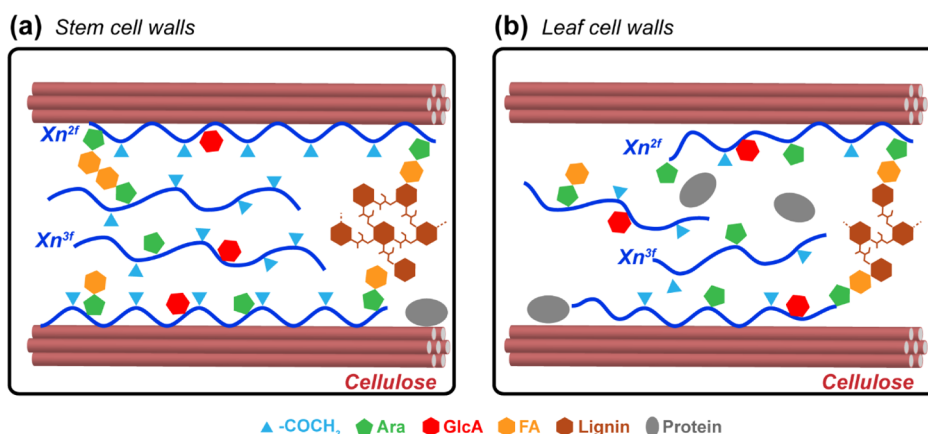


Figure 8. Schematic models of the *Brachypodium* stem (a) and leaf (b) cell walls. The stem has a higher concentration of acetylated and ferulated Xn^{2f} compared to the leaf cell wall. These acetylated Xn^{2f} chains interact more strongly with cellulose fibrils and are more rigid in the stem than in the leaf cell wall. Xn^{3f} chains are more disordered than Xn^{2f} and reside mostly in the interfibrillar space.

DISCUSSION

The current study extends our previous analysis of *B. distachyon* seedling PCWs by comparing whole-cell samples of the mature stem, leaf, and roots grown in light. In this way, we obtain information about how the developmental stage and secondary cell wall content change the xylan concentration, functionalization, dynamics, and interaction with other wall polysaccharides. Quantitative ^{13}C NMR spectra (Figure 2) and 2D *J*-INADEQUATE spectra (Figure 4) indicate that the stem and leaf cell walls, as compared to seedling PCWs, contain less arabinose, less branched arabinan, and less terminal arabinose on GAX side chains. No xyloglucan is detected in the stem and leaf cell walls, in contrast to the seedling PCW, which contains a moderate amount of xyloglucan.²⁴ Thus, the stem and leaf cell walls have much lower concentrations of non-xylan matrix polysaccharides than seedling. Instead, the quantitative ^{13}C spectra show that the stem and leaf samples contain either more or similar amounts of xylan compared to seedling PCWs. Between the stem and leaf, the stem has $\sim 20\%$ more total xylan than the leaf, and the xylan in the stem is more acetylated. The higher amount of xylan in the stem than in the leaf is consistent with the hypothesis that GAX participates in the linkage between cellulose and lignin,¹⁹ as the thicker secondary cell wall of the stem would require a larger amount of GAX to bridge these two polymers. The CP-INADEQUATE spectra show that the amount of the rigid Xn^{2f} is 3 times higher in the stem than in the leaf cell wall, consistent with the hypothesis that GAX adopts a twofold conformation to bind to cellulose fibrils.¹¹

The 1-s 2D CC spectra allow us to probe the side-chain decoration of xylan. The spectra indicate that xylan in the stem is more acetylated and ferulated than that in the leaf. Since stem contains 20% more total xylan than the leaf (Figures 5c and 6c), and the acetylated xylan intensities are ~ 2.5 -fold higher for the stem than those for the leaf (Figure 6c); these values indicate an approximately 2-fold higher acetylation level for xylan in the stem than in the leaf cell wall. We can also estimate the absolute acetylation levels by considering the relative intensities of the (82, 21) and (103, 21) ppm cross peaks in the 1 s 2D ^{13}C spin diffusion spectra. Assuming the acetyl methyl group and the xylan backbone have reached equilibrium within 1 s of spin diffusion, the intensity ratio between the 21 ppm cross peak ($COOCH_3$) and the diagonal

peak in the 82 ppm Xn^{2f} C4 cross section represents the acetylation level of twofold xylan. Likewise, the intensity ratio between the 21 ppm cross peak and the diagonal peak in the 103 ppm Xn^{3f} C1 cross section represents the threefold xylan acetylation level. Spectral integration indicates that the intensity ratio is 0.30 for Xn^{2f} and 0.25 for Xn^{3f} in the stem. For the leaf, these ratios are much lower, at ~ 0.08 for Xn^{2f} and ~ 0.07 for Xn^{3f} , and have larger uncertainties. However, magnetization transfer between the acetyl and xylan backbone is not fully equilibrated. This is shown by the intensity ratio of 0.75:1 between the 170 ppm acetyl C=O peak and the 21 ppm acetyl methyl peak in the 21 ppm cross section, instead of the 1:1 ratio expected for fully equilibrated magnetization transfer (Figure 6c). Correcting for this incomplete equilibration, we obtain an acetylation level of at least 40% for Xn^{2f} and at least 33% for Xn^{3f} in the stem cell wall. The minimum 40% acetylation level of Xn^{2f} is in good agreement with mass spectrometry data of *Arabidopsis* secondary cell walls, which showed that xylosyl residues are alternatingly acetylated at the O-2/3 positions.¹¹ Since the acetylation level of the leaf is about 2-fold lower compared to that of the stem, we estimate values of $\sim 20\%$ for Xn^{2f} and $\sim 15\%$ for Xn^{3f} . The higher xylan acetylation level in the stem should promote xylan to form the twofold symmetric conformation to bind the cellulose microfibril. This prediction is confirmed by the stronger cross peak between Xn^{2f} and surface cellulose (Figure 6). This stronger Xn^{2f} -cellulose interaction also explains the higher xylan intensities in the CP-INADEQUATE spectrum of the stem compared to that of the leaf. A recent solid-state NMR study of the switchgrass stem detected Xn^{3f} but not Xn^{2f} . It was suggested that grass xylan may have side-chain decorations incompatible with binding to cellulose in the Xn^{2f} conformation and that this Xn^{2f} conformation may arise only after dehydration.³⁷ The present study on never-dried *Brachypodium* tissues confirms that some xylan in grasses does indeed have branches that permit binding to cellulose in the Xn^{2f} conformation.¹⁶


Both twofold and threefold xylan chains are more rigid in the stem and leaf cell walls than in the seedling PCW, as manifested by the absence of its cross peaks in the *J*-INADEQUATE spectra. DIPSHIFT data (Figure 7) further reveal that Xn^{2f} is more rigid in the stem than in the leaf. It is noteworthy that almost every polysaccharide in the stem and leaf cell walls is more rigid than in the seedling PCW,²⁴ as

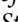
shown by DIPSHIFT data and the loss of *J*-INADEQUATE peak intensities for the stem and leaf samples. The seedling PCW studied previously was mildly extracted to remove proteins and lipids.²⁴ However, since extraction removes more soluble and mobile chemical species than recalcitrant components, it is likely that all wall polysaccharides are inherently more immobilized in secondary cell walls than in PCWs.

The current comparisons of the chemical composition, dynamics, and interactions of polysaccharides in the *Brachypodium* stem and leaf whole cells lead to the following structural model of xylan's role in promoting the secondary cell wall structure (Figure 8). Compared to the leaf, the stem cell wall contains more cellulose and xylan, and the xylan chains are about 2 times more acetylated and 60% more ferulated. The ~40% acetylation of Xn^{2f} in the stem not only immobilizes the xylan chain, which explains the DIPSHIFT data and the *J*-INADEQUATE data, but more importantly, also increases xylan binding to cellulose in the stem compared to the less acetylated leaf cell wall. We propose that this increased xylan–cellulose interaction in turn bridges cellulose–lignin association, which is central to the formation of the thicker and more mature secondary cell wall. When the xylan acetylation level is low, as seen in the leaf cell wall, then GAX has less propensity to “zip up” into the twofold screw conformation to pack onto the cellulose surface. This may in turn inhibit the cellulose–lignin association that is necessary for secondary wall formation. Therefore, xylan acetylation may be a key chemical event in the formation and resulting structural characteristics of secondary cell walls.

AUTHOR INFORMATION

Corresponding Authors

Paul Dupree – Department of Biochemistry, University of Cambridge, Cambridge CB2 1QW, U.K.;  orcid.org/0000-0001-9270-6286; Email: pd101@cam.ac.uk

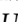
Mei Hong – Department of Chemistry, Massachusetts Institute of Technology, Cambridge, Massachusetts 02139, United States;  orcid.org/0000-0001-5255-5858; Email: meihong@mit.edu

Authors

Pu Duan – Department of Chemistry, Massachusetts Institute of Technology, Cambridge, Massachusetts 02139, United States;  orcid.org/0000-0002-7395-4353

Samuel J. Kaser – Department of Chemistry, Massachusetts Institute of Technology, Cambridge, Massachusetts 02139, United States

Jan J. Lyczakowski – Department of Biochemistry, University of Cambridge, Cambridge CB2 1QW, U.K.; Present Address: Department of Plant Biotechnology, Faculty of Biochemistry, Biophysics and Biotechnology, Jagiellonian University, Gronostajowa 7, 30-387 Krakow, Poland.

Pyaee Phyoo – Department of Chemistry, Massachusetts Institute of Technology, Cambridge, Massachusetts 02139, United States;  orcid.org/0000-0002-3019-6011

Theodora Tryfona – Department of Biochemistry, University of Cambridge, Cambridge CB2 1QW, U.K.

Complete contact information is available at:

<https://pubs.acs.org/10.1021/acsomega.1c01978>

Notes

The authors declare no competing financial interest.

ACKNOWLEDGMENTS

This research was supported by the Center for Lignocellulose Structure and Formation, an Energy Frontier Research Center funded by the U.S. Department of Energy, Office of Science, Basic Energy Sciences under award # DE-SC0001090.

REFERENCES

- (1) Ragauskas, A. J.; Williams, C. K.; Davison, B. H.; Britovsek, G.; Cairney, J.; Eckert, C. A.; Frederick, W. J.; Hallett, J. P.; Leak, D. J.; Liotta, C. L.; Mielenz, J. R.; Murphy, R.; Templer, R.; Tschaplinski, T. The path forward for biofuels and biomaterials. *Science* **2006**, *311*, 484–489.
- (2) Service, R. F. Cellulosic ethanol - Biofuel researchers prepare to reap a new harvest. *Science* **2007**, *315*, 1488.
- (3) McCann, M.; Carpita, N. Designing the deconstruction of plant cell walls. *Curr. Opin. Plant Biol.* **2008**, *11*, 314–320.
- (4) Scheller, H. V.; Ulvskov, P. Hemicelluloses. *Annu. Rev. Plant Biol.* **2010**, *61*, 263–289.
- (5) Initiative, I. B. Genome sequencing and analysis of the model grass *Brachypodium distachyon*. *Nature* **2010**, *463*, 763–768.
- (6) Iiyama, K.; Lam, T. B. T.; Stone, B. A. Phenolic acid bridges between polysaccharides and lignin in wheat internodes. *Phytochemistry* **1990**, *29*, 733–737.
- (7) Coomey, J. H.; Sibout, R.; Hazen, S. P. Grass secondary cell walls, *Brachypodium distachyon* as a model for discovery. *New Phytol.* **2020**, *227*, 1649–1667.
- (8) Rancour, D. M.; Marita, J. M.; Hatfield, R. D. Cell wall composition throughout development for the model grass *Brachypodium distachyon*. *Front. Plant Sci.* **2012**, *3*, 266.
- (9) Hatfield, R. D.; Ralph, J. Modelling the feasibility of intramolecular dehydrodiferulate formation in grass walls. *J. Sci. Food Agric.* **1999**, *79*, 425–427.
- (10) Saeman, J. F.; Moore, W. E.; Millett, M. A. Sugar Units Present: Hydrolysis and Quantitative Paper Chromatography. In *Methods in Carbohydrate Chemistry*; Whistler, R. L., Ed.; Academic Press: New York, 1963; pp 54–69.
- (11) Busse-Wicher, M.; Gomes, T. C.; Tryfona, T.; Nikolovski, N.; Stott, K.; Grantham, N. J.; Bolam, D. N.; Skaf, M. S.; Dupree, P. The pattern of xylan acetylation suggests xylan may interact with cellulose microfibrils as a twofold helical screw in the secondary plant cell wall of *Arabidopsis thaliana*. *Plant J.* **2014**, *79*, 492–506.
- (12) Nieduszynski, I.; Marchessault, R. H. Structure of beta-D-(1→4')xylan hydrate. *Nature* **1971**, *232*, 46–47.
- (13) Simmons, T. J.; Mortimer, J. C.; Bernardinelli, O. D.; Pöppler, A.-C.; Brown, S. P.; deAzevedo, E. R.; Dupree, R.; Dupree, P. Folding of xylan onto cellulose fibrils in plant cell walls revealed by solid-state NMR. *Nat. Commun.* **2016**, *7*, 13902.
- (14) Dupree, R.; Simmons, T. J.; Mortimer, J. C.; Patel, D.; Iuga, D.; Brown, S. P.; Dupree, P. Probing the molecular architecture of *Arabidopsis thaliana* secondary cell walls using two- and three-dimensional ¹³C solid state nuclear magnetic resonance spectroscopy. *Biochemistry* **2015**, *54*, 2335–2345.
- (15) Jaafar, Z.; Mazeau, K.; Boissière, A.; Le Gall, S.; Villares, A.; Vigouroux, J.; Beury, N.; Moreau, C.; Lahaye, M.; Cathala, B. Meaning of xylan acetylation on xylan–cellulose interactions: A quartz crystal microbalance with dissipation (QCM-D) and molecular dynamic study. *Carbohydr. Polym.* **2019**, *226*, 115315.
- (16) Kang, X.; Kirui, A.; Dickwella Widanage, M. C.; Mentink-Vigier, F.; Cosgrove, D. J.; Wang, T. Lignin–polysaccharide interactions in plant secondary cell walls revealed by solid-state NMR. *Nat. Commun.* **2019**, *10*, 347.
- (17) Reif, B.; Ashbrook, S. E.; Emsley, L.; Hong, M. Solid-state NMR spectroscopy. *Nat. Rev. Methods Primers* **2021**, *1*, 2.
- (18) Wang, T.; Park, Y. B.; Cosgrove, D. J.; Hong, M. Cellulose–Pectin Spatial Contacts Are Inherent to Never-Dried *Arabidopsis* Primary Cell Walls: Evidence from Solid-State Nuclear Magnetic Resonance. *Plant Physiol.* **2015**, *168*, 871–884.

- (19) Dick-Pérez, M.; Zhang, Y.; Hayes, J.; Salazar, A.; Zabolina, O. A.; Hong, M. Structure and interactions of plant cell-wall polysaccharides by two- and three-dimensional magic-angle-spinning solid-state NMR. *Biochemistry* **2011**, *50*, 989–1000.
- (20) White, P. B.; Wang, T.; Park, Y. B.; Cosgrove, D. J.; Hong, M. Water–Polysaccharide Interactions in the Primary Cell Wall of *Arabidopsis thaliana* from Polarization Transfer Solid-State NMR. *J. Am. Chem. Soc.* **2014**, *136*, 10399–10409.
- (21) Phyo, P.; Gu, Y.; Hong, M. Impact of acidic pH on plant cell wall polysaccharide structure and dynamics: insights into the mechanism of acid growth in plants from solid-state NMR. *Cellulose* **2019**, *26*, 291–304.
- (22) Phyo, P.; Wang, T.; Kiemle, S. N.; O'Neill, H.; Pingali, S. V.; Hong, M.; Cosgrove, D. J. Gradients in Wall Mechanics and Polysaccharides along Growing Inflorescence Stems. *Plant Physiol.* **2017**, *175*, 1593–1607.
- (23) Bromley, J. R.; Busse-Wicher, M.; Tryfona, T.; Mortimer, J. C.; Zhang, Z.; Brown, D. M.; Dupree, P. GUX1 and GUX2 glucuronyltransferases decorate distinct domains of glucuronoxylan with different substitution patterns. *Plant J.* **2013**, *74*, 423–434.
- (24) Wang, T.; Salazar, A.; Zabolina, O. A.; Hong, M. Structure and Dynamics of Brachypodium Primary Cell Wall Polysaccharides from Two-Dimensional ¹³C Solid-State Nuclear Magnetic Resonance Spectroscopy. *Biochemistry* **2014**, *53*, 2840–2854.
- (25) Wang, T.; Phyo, P.; Hong, M. Multidimensional solid-state NMR spectroscopy of plant cell walls. *Solid State Nucl. Magn. Reson.* **2016**, *78*, 56–63.
- (26) Bennett, A. E.; Rienstra, C. M.; Auger, M.; Lakshmi, K. V.; Griffin, R. G. Heteronuclear decoupling in rotating solids. *J. Chem. Phys.* **1995**, *103*, 6951–6958.
- (27) Elena, B.; Lesage, A.; Steuernagel, S.; Böckmann, A.; Emsley, L. Proton to Carbon-13 INEPT in Solid-State NMR Spectroscopy. *J. Am. Chem. Soc.* **2005**, *127*, 17296–17302.
- (28) Hohwy, M.; Rienstra, C. M.; Jaroniec, C. P.; Griffin, R. G. Fivefold symmetric homonuclear dipolar recoupling in rotating solids: Application to double quantum spectroscopy. *J. Chem. Phys.* **1999**, *110*, 7983–7992.
- (29) Cadars, S.; Sein, J.; Duma, L.; Lesage, A.; Pham, T. N.; Baltisberger, J. H.; Brown, S. P.; Emsley, L. The refocused INADEQUATE MAS NMR experiment in multiple spin-systems: Interpreting observed correlation peaks and optimising lineshapes. *J. Magn. Reson.* **2007**, *188*, 24–34.
- (30) Hou, G.; Yan, S.; Trébosc, J.; Amoureux, J.-P.; Polenova, T. Broadband homonuclear correlation spectroscopy driven by combined R2nv sequences under fast magic angle spinning for NMR structural analysis of organic and biological solids. *J. Magn. Reson.* **2013**, *232*, 18–30.
- (31) Munowitz, M. G.; Griffin, R. G.; Bodenhausen, G.; Huang, T. H. Two-dimensional rotational spin-echo NMR in solids: correlation of chemical shift and dipolar interactions. *J. Am. Chem. Soc.* **1981**, *103*, 2529–2533.
- (32) Hong, M.; Gross, J. D.; Rienstra, C. M.; Griffin, R. G.; Kumashiro, K. K.; Schmidt-Rohr, K. Coupling Amplification in 2D MAS NMR and Its Application to Torsion Angle Determination in Peptides. *J. Magn. Reson.* **1997**, *129*, 85–92.
- (33) Bielecki, A.; Kolbert, A. C.; Levitt, M. H. Frequency-switched pulse sequences: homonuclear decoupling and dilute spin NMR in solids. *Chem. Phys. Lett.* **1989**, *155*, 341–346.
- (34) Huster, D.; Xiao, L.; Hong, M. Solid-state NMR investigation of the dynamics of the soluble and membrane-bound colicin Ia channel-forming domain. *Biochemistry* **2001**, *40*, 7662–7674.
- (35) Grantham, N. J.; Wurman-Rodrich, J.; Terrett, O. M.; Lyczakowski, J. J.; Stott, K.; Iuga, D.; Simmons, T. J.; Durand-Tardif, M.; Brown, S. P.; Dupree, R.; Busse-Wicher, M.; Dupree, P. An even pattern of xylan substitution is critical for interaction with cellulose in plant cell walls. *Nat. Plants* **2017**, *3*, 859–865.
- (36) Wang, T.; Hong, M. Solid-state NMR investigations of cellulose structure and interactions with matrix polysaccharides in plant primary cell walls. *J. Exp. Bot.* **2016**, *67*, 503–514.
- (37) Gao, Y.; Lipton, A. S.; Wittmer, Y.; Murray, D. T.; Mortimer, J. C. A grass-specific cellulose-xylan interaction dominates in sorghum secondary cell walls. *Nat. Commun.* **2020**, *11*, 6081.